

# DESIGN AND INITIAL COMMISSIONING OF BEAM DIAGNOSTICS FOR THE KEK COMPACT ERL

R. Takai<sup>#</sup>, T. Obina, H. Sagehashi, Y. Tanimoto, T. Honda, T. Nogami, M. Tobiya, KEK, 1-1 Oho, Tsukuba, Ibaraki 305-0801, Japan

## Abstract

A compact energy-recovery linac (cERL) was constructed at KEK as a test accelerator for the ERL-based light source. Standard beam monitors such as beam position monitors (BPMs), screen monitors (SCMs), and beam loss monitors (BLMs) have been developed for the cERL and used in its commissioning. For the main BPMs, we adopted the stripline type, the time response of which is improved by using a glass-sealed feedthrough. The SCMs are equipped with two types of screens and an RF shield for wake-field suppression. Optical fibers with photomultiplier tubes (PMTs), covering the entire cERL circumference, are used as the BLM. CsI scintillators with large-cathode PMTs are also prepared for detecting local beam loss. The design and some initial commissioning results of these standard monitors are described in this paper.

## INTRODUCTION

The energy-recovery linac (ERL) has recently received significant attention as one of the promising candidates for next-generation light sources [1]. The Compact ERL (cERL), which is a test accelerator aimed at demonstrating the key technologies for the ERL-based light source, was constructed at KEK, and the complete system was commissioned in December 2013. The commissioning proceeded without troubles, and we successfully accelerated 6.5- $\mu$ A CW beams to energies reaching 20 MeV; the beams recirculated without major loss, and they were guided to the beam dump after energy recovery in only two months [2]. In such an early phase of commissioning, standard beam diagnostics such as the monitoring of beam position, beam profile, and beam loss plays a central role. In this paper, we describe the design of our standard beam monitors that have contributed to

the efficient cERL commissioning, and we report the initial commissioning results.

The beam monitors used for the cERL are listed in Table 1, and Fig. 1 shows their schematic layout. Four sets of fiber loss monitors cover the entire cERL circumference. Because the CsI-scintillator-based beam loss monitors described later are still under development, they are not listed in Table 1. Four current transformers (CTs) and a DCCT are currently not used, because of the low beam current. The beam current is measured by using not only the three movable Faraday cups (FCs) listed in Table 1 but also two beam dumps: injector and main dumps. In addition to these monitors, a slit scanner and a deflecting cavity are installed along the diagnostic line following the injector for the emittance and bunch-length measurements, respectively [3].

Table 1: List of cERL Beam Monitors

Monitor Type	Objective	#
BPM (Stripline/Button)	Position, Charge	45
SCM (Ce:YAG/OTR)	Position, Profile	30
BLM (Fiber&PMT)	Loss	4
CT	Charge	4
DCCT	Current	1
Movable FC	Charge	3

## BEAM POSITION MONITOR

A beam position monitor (BPM) is a very useful tool especially for monitoring high-intensity ERL beams because it can non-destructively measure the beam centroid displacement in the transverse plane. The cERL has 45 BPMs, which are roughly classified into five types according to the duct structure and electrode type. This section describes the design of the BPM duct in the straight section, which contains the largest number of

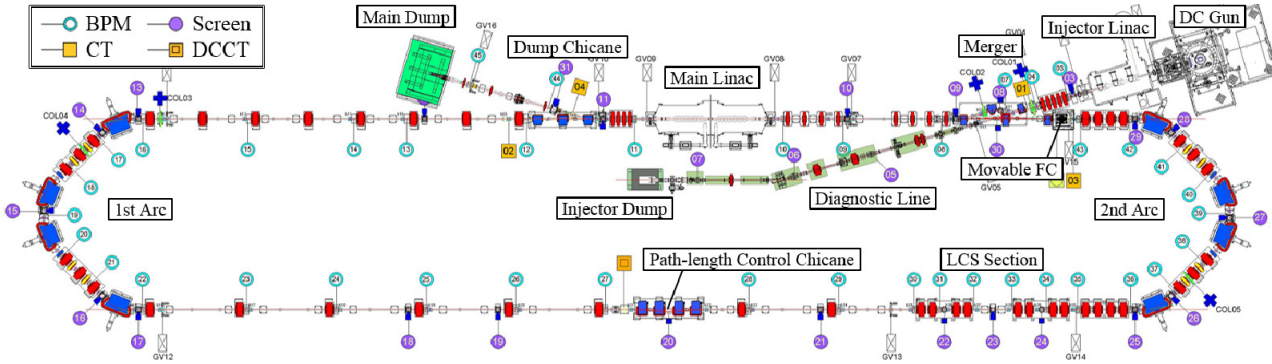


Figure 1: Layout of cERL beam monitors.

<sup>#</sup>ryota.takai@kek.jp

BPMs, and its electronics used for detecting the beam signals. To demonstrate the use of BPMs in the commissioning, we also report the result of measuring two-color beams before and after the circulation for energy recovery.

### Design of the BPM Duct

Figure 2(a) shows a schematic of the BPM duct in the straight section. Stripline electrodes are disposed on the top and bottom as well as right and left inner walls of the duct, which has an inner diameter of 50 mm. The length of each electrode was fixed as 28.8 mm to maximize sensitivity to the frequency component of 2.6 GHz, which is the beam's maximal repetition frequency. As for BPMs installed along the injector line and the dump line where the repetition frequency is only 1.3 GHz even when future upgrades are considered, the electrode length was set to 57.6 mm, which is twice the length of the above electrodes. The electrode width was selected such that the opening angle relative to the beam axis is 20° for all BPMs. The characteristic impedance of each electrode was designed to be  $50 \Omega$ , and it was confirmed using time domain reflectometry (TDR). The electrode end at the downstream side was directly welded to the duct wall and grounded. Beam signals induced on the electrode are extracted to the outside through a feedthrough welded at the upstream side end of the electrode. In this feedthrough, low-permittivity glass (BHA,  $\epsilon_r = 5.0$ ) is used for insulation and sealing to improve the time response [4]. The wake fields excited by the beam and the beam coupling impedance were evaluated in advance by using GdfidL [5]. In the simulations of an electron beam with a bunch length of 1 mm (3.3 ps), the longitudinal loss factor was calculated to be 59.1 mV/pC. After conversion into the power loss for the beam average current of 10 mA, the loss factor becomes 4.6 mW. For vacuum flanges at both ends of the BPM duct, we used special gapless and stepless flanges developed to reduce the wake fields [6]. A cylindrical boss on the top surface is useful for precise alignment because it can be used to mount a level and a reflection target of the laser tracker on the duct. Figure 2(b) shows a photograph of the stripline electrodes inside the BPM duct.

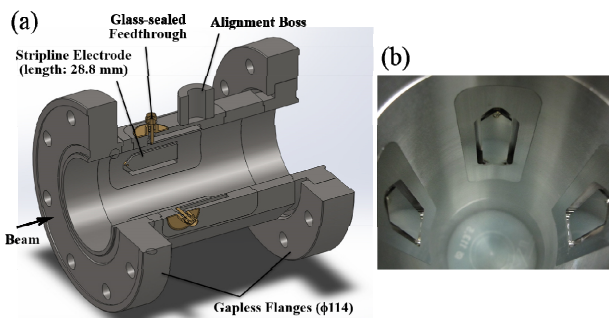


Figure 2: (a) Schematic drawing of the BPM duct in the straight section. (b) Photograph of the stripline electrodes taken from the upstream side.

### Detection Circuit & Digitizer

BPMs for the ERL require a broad dynamic range rather than high measurement accuracy. Therefore, we adopted a log detection circuit with a bandwidth of 10 MHz to detect the beam signals. Although the preferable center frequency for wave detection with noise reduction is 2.6 GHz, it was taken to be 1.3 GHz because the cut-off frequency of the octagonal duct in the arc section is approximately 2.6 GHz. The block diagram of the detection circuit is shown in Fig. 3. Output signals from one BPM are processed in one NIM module including four detection circuits. When a variable attenuator following an input port is set to 0 dB, the detection circuit log-linearly responds to the input voltage in the range of -90 to -30 dBm. The rise time of the output signals for a pulse input of width 1  $\mu$ s is about 200 ns. A commercial high-speed data acquisition unit and insulating input modules were employed as a digitizer (Yokogawa, SL1000). This digitizer has a sufficiently wide analog bandwidth and a resolution of 12 bit. It can be utilized for beam current monitoring by inputting the output signal of a Faraday cup, in addition to other waveform analyses.

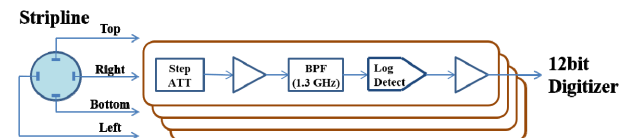


Figure 3: Block diagram of the detection circuit.

### Examples of BPM Usage

Beam positions measured by the BPM are shown in Fig. 4(a) in red as a function of time. In this experiment, we changed the beam position stepwise by using a steering magnet located upstream from the BPM. The blue line indicates the nominal beam positions calculated on the basis of the measurement obtained using a screen monitor. The two measurements are in a good agreement. If the BPM resolution, including the beam position jitter, is evaluated from the variation of the measurement data, the obtained value is about 150  $\mu$ m. Figure 4(b) shows the mapping results calculated using CST PARTICLE STUDIO [7]. The sensitivity curve obtained by fitting the fifth degree polynomial to this map was used for converting the detected signal into the beam position.

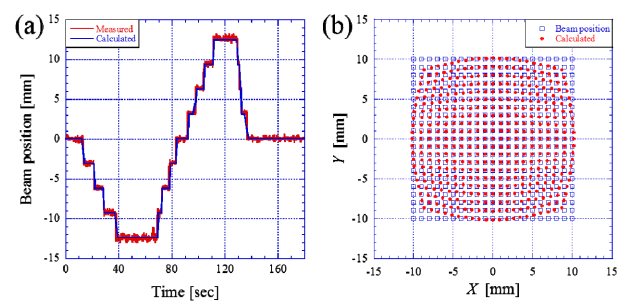


Figure 4: (a) Comparison of beam positions measured by the BPM with those obtained using a screen monitor. (b) BPM mapping results.

In the section between the merger and the dump chicane, destructive monitors such as screen monitors cannot be used to observe the post-circulation high-energy beam, because the pre-circulation low-energy beam is simultaneously propagating in the same section. Therefore, we focused on the fact that the post-circulation beam signals superimpose on the pre-circulation signals with a constant delay corresponding to the circulation time, and we devised a simple method to detect the positions of these beams individually by using a BPM. This method is schematically illustrated in Fig. 5(a). In the case of burst mode with macro-pulse beams that is commonly used in the commissioning, the head and tail parts of the detected signal contain only pre- and post-circulation beam signals, respectively, because of the above delay. Ideally, there are no signals between these parts because the 2.6-GHz component produced by the superimposition of the beam signals dephased by  $180^\circ$  relative to each other for the energy recovery is removed by the bandpass filter in the detection circuit. Figure 5(b) shows the measurement results of the two-color beams obtained upstream and downstream of the main linac. Each detected signal from four circuits has a step-like profile, and we can clearly distinguish the two different energy beams. The width of each part depends on the beam's circulation time, which for the cERL is about 300 ns. The difference between the rise times of detected signals is caused by the characteristic difference between the detection circuits used in this measurement. The reason for the appearance of finite signals between these parts is that the phase difference of  $180^\circ$  shifts in proportion to the distance from the main linac because of the beam energy difference. In other words, the signals in this part can be used as a beam phase monitor. This simple and reliable method worked very well in adjusting

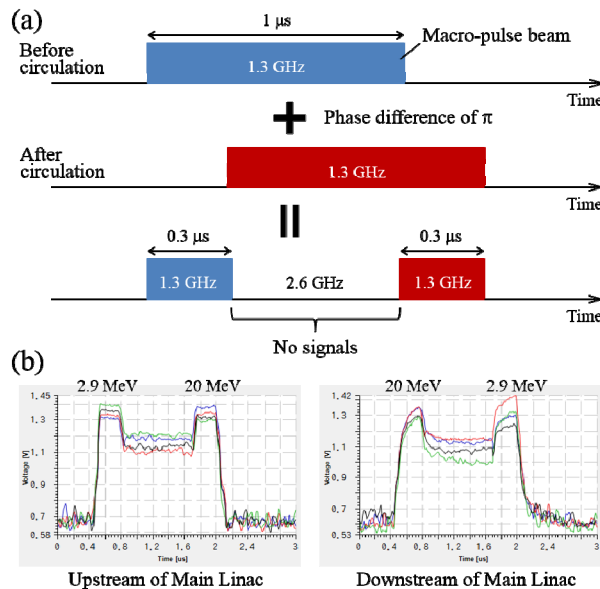


Figure 5: (a) Schematic of the measurement of two-color beams by using a BPM. (b) Measurement results obtained upstream and downstream of the main linac.

the beam orbit after the circulation. If a negligible blank area with no beam is added periodically, this method can be applied to the CW beams.

## SCREEN MONITOR

While a screen monitor (SCM) is a typical destructive monitor, it is one of the essential instruments, especially for the linac commissioning, because it enables the precise measurement of the beam position and profile even for low-intensity beams. The SCM is also useful for estimating the beam quality by combining it with a magnet or a deflecting cavity located upstream of it. As shown in Fig. 1, 30 SCMs are present in the cERL. The internal structure of the SCM differs depending on the installation section and can be classified into six types. In this section, we describe the details of the SCM installed in the straight section and report the emittance measurement results obtained by using it.

### Design of the SCM Duct

A schematic of the SCM duct in the straight section and a photograph of the screen holder are shown in Fig. 6. The duct's internal structure was designed on the basis of that employed at JLab and BNL [8, 9]. The two-stage screen holder allows us to use two different screens according to the beam energy and intensity. The first screen is a 100-μm-thick Ce:YAG scintillator. The beam is normally incident on the scintillator's surface. Fluorescent light emitted from the scintillator is guided to a side viewport through a thin SUS mirror arranged at  $45^\circ$  relative to the beam axis. The beam incidence surface is coated with a 3-nm-thick aluminum layer to avoid damage due to charge-up. The second screen is a metal foil used for generating an optical transition radiation (OTR). We adopted an aluminum-coated silicon wafer as the OTR radiator so that the radiation surface is flat. The thickness of the wafer and coating are 70 μm and 40 nm, respectively. To prevent overlapping of the forward OTR emitted from the wafer's rear surface and the backward OTR emitted from the mirror's front surface, this screen was arranged at  $45^\circ$  relative to the beam axis. Both apertures of these screens are 28 mm in diameter. Four

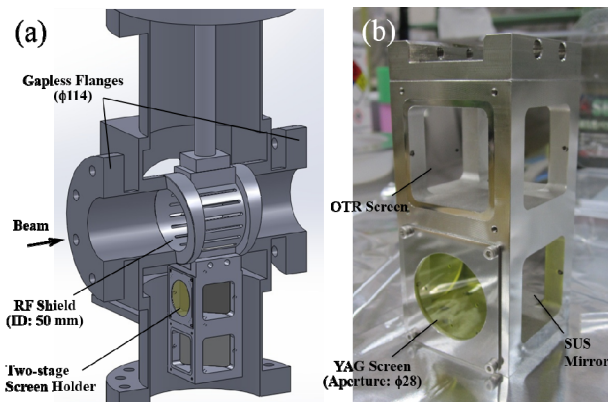


Figure 6: (a) Schematic of the SCM duct in the straight section. (b) Photograph of the two-stage screen holder.

holes of diameter 1 mm each are located at peripheral parts of the screens and used for the focus adjustment and the magnification calibration for the imaging optics. These screens are concealed behind a cylindrical RF shield when not in use. The RF shield is smoothly connected with the adjacent beam ducts only with physical contact through high-precision fitting. According to the GdfidL estimation, this RF shield reduces the longitudinal loss factor to 1/100 (10 mV/pC) or below for an electron beam with 1-mm bunch length. These components are driven by a pneumatic actuator with a positioning precision of 0.1 mm or less. As in the BPM duct, gapless flanges are also used for the SCM duct.

### *Imaging Optics & CCD Camera*

As mentioned above, the light emitted from the screen is extracted in the direction perpendicular to the beam axis and then relayed via an optical window and a flat mirror to a CCD camera (Allied Vision Technologies, Prosilica GC650). The flat mirror in the middle of the optical path is useful for adjusting the optical axis and protecting the camera from radiation-induced damage. A low-distortion CCTV lens with a diaphragm is mounted on the camera's front (Myutron, HS5028J3). Figure 7 shows a focused image of a calibration pattern obtained using the imaging optics with a magnification that is actually used in the commissioning. The spatial resolution of the YAG screen was estimated by accounting for the depth of field and multiple scattering of electrons in the Ce:YAG crystal in addition to the edge width of this image. Assuming the image bleeding to be on the order of the crystal's thickness, the spatial resolution was estimated to be 62  $\mu\text{m}$ . Because the OTR screen is not affected by the multiple scattering of electrons, it is expected that the resolution is improved up to about 40  $\mu\text{m}$ .

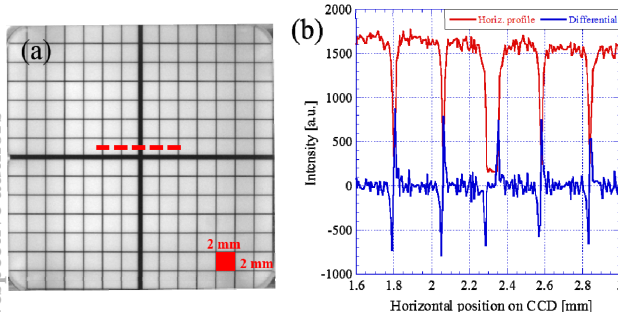


Figure 7: (a) Focused image of the calibration pattern. (b) Horizontal profile on the dashed line and its position differential.

### *Examples of SCM Usage*

Thus far, we primarily used the YAG screen in the commissioning with low-energy and low-intensity beams. The linearity of the fluorescence intensity in the range of beam densities achieved in the commissioning was confirmed experimentally in advance. The exposure time of the camera was typically set to 100  $\mu\text{s}$ . In this setup,

noise signals caused by a dark current emitted from the superconducting cavities tuned for the acceleration up to 20 MeV were negligibly small.

The beam tuning effect clearly appears in the beam's normalized emittance. It was measured by employing the quadrupole-scan (Q-scan) method using the SCM. An example of the Q-scan result acquired at the downstream section of the first arc is shown in Fig. 8. The bunch charge was approximately 20 fC/bunch. The space charge effect in the bunch can be negligible. The quadrupole magnet used for the measurement, in other words the length of the drift space between the quadrupole magnet and the SCM, was selected such that the beam size at the waist position of the graph was not lower than the spatial resolution of the YAG screen. The camera's gain and the density of ND filters were adjusted carefully to prevent the saturation of CCD pixels even at the waist position. The normalized emittance can be calculated from some coefficients obtained by fitting the theoretical function to these measurement data by using the weighted least squares method. Although the initial emittance was over 0.4 mm·mrad in both horizontal and vertical directions, it gradually reduced as the beam tuning proceeded and reached the value of 0.14 mm·mrad. This was almost the same as the design value for low-bunch-charge beams. In the latter part of the commissioning, the normalized emittance for high bunch charge (7.7 pC/bunch) was also measured by employing the same method. While the measured value is still larger than the target value at present, it is decreasing steadily because of elaborate optics matching using the SCM.

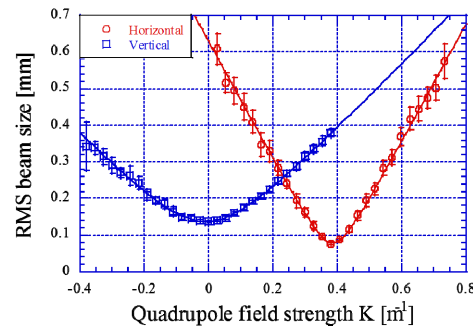


Figure 8: Example of the emittance measurement using the Q-scan method (for a low bunch charge of ~20 fC/bunch).

## **BEAM LOSS MONITOR**

### *Fast Beam Loss Monitors*

Throughout the commissioning, typical beam tuning was performed with a 1- $\mu\text{s}$  macro-pulse beam with 20 fC/bunch and 770-ps (1.3 GHz) bunch spacing. Because the electron source of the cERL is a 500-kV DC photocathode gun, high-charge beams with pulse length greater than expected may be produced in the case of a trouble of the laser. To avoid serious damage to screen monitors or other accelerator components, it is essential to

have a fast interlock system for stopping the gun laser by using beam loss monitors (BLMs). The first goal of our fast BLM is to attain time response on the order of 1  $\mu$ s.

Four 30-m long optical fibers were installed along the vacuum chamber as one of the fast BLMs, covering the entire cERL circumference [10]. Photomultiplier tubes (PMTs, Hamamatsu, H10721-110) were attached at both ends of the fiber, and two oscilloscopes were used to analyze the time structure of the output signal. This monitor is primarily used to estimate the beam-loss point along the circumference.

We have also developed a fast BLM by using a pure CsI crystal for local beam loss detection [11]. The dimensions of the CsI crystal are 10 mm  $\times$  10 mm  $\times$  25 mm, and it is attached to a large-size PMT cathode (Hamamatsu, R11558). Figure 9(a) shows an example of beam loss detection at the first arc section. The green and blue lines indicate output signals of the PMT with a CsI scintillator and of a post-stage integration circuit for the interlock system, respectively. A time response sufficiently fast for detecting 1- $\mu$ s-wide macro pulses is clearly obtained. Note that this measurement was performed before the precise optics matching, and the signal was caused by a loss of the beam's tail. When the beam's core is lost (e.g., when the screen is inserted), the output signal voltage is much higher than that shown in Fig. 9(a). After matching the arc section optics, the beam loss drastically decreased, as shown in Fig. 9(b). Since a thallium-doped CsI crystal has longer time response but higher sensitivity, it will also be utilized for small beam loss detection.

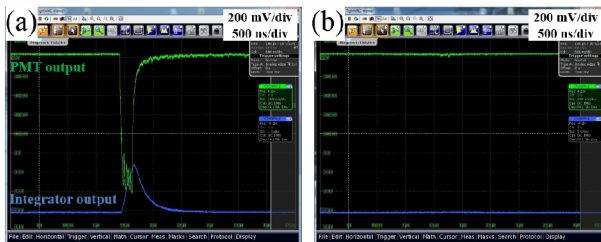


Figure 9: Example of beam loss detection at the first arc section. Before (a) and after (b) the optics matching.

### Slow Radiation Monitors

Twelve area monitors were used to measure the gamma dose rate inside the accelerator shield. As a second-order time response is sufficient for this purpose, we adopted ALOKA MAR-782, which utilizes a silicon semiconductor detector to measure gamma rays with energies ranging from 50 keV to 6 MeV. Each area monitor can be arbitrarily set at a threshold level of interlock for stopping the gun laser. A 4-port RS232 device server embedded with EPICS was developed to remotely observe the radiation levels measured by each area monitor [12], and it worked without troubles for over half a year.

Low-energy gamma rays with energies above 7 keV were primarily detected using an ion chamber survey

meter, Fluke 451B, which was also used to cut off the gun's high voltage when the radiation dose exceeded a threshold level.

### SUMMARY AND FUTURE PLAN

The details of BPMs, SCMs, and BLMs for the cERL, which are the most standard and the most important beam monitors, were described. Commissioning toward the experimental utilization of pulsed X-rays generated by laser Compton scattering (LCS) will start in January 2015. By that time, we plan to add two button-type BPMs at both sides of the LCS collision point and a large-aperture SCM at the dump line. In addition, we are also preparing for bunch-length measurement using coherent transition radiation and a Michelson interferometer to confirm the effect of bunch compression with the first arc [13].

### ACKNOWLEDGMENT

The authors would like to thank all members of the cERL commissioning team for their collaborative efforts during this work. We would also like to thank T. Michikawa and H. Kameta for their continuing support in the construction of the control system for beam monitors and other components.

### REFERENCES

- [1] N. Nakamura, "Review of ERL Projects at KEK and around the World," IPAC'12, New Orleans, p. 1040 (2012).
- [2] S. Sakanaka et al., "The First Beam Recirculation and Beam Tuning in the Compact ERL at KEK," LINAC'14, Geneva, TUPP075 (2014).
- [3] S. Sakanaka et al., "Construction and Commissioning of the Compact-ERL Injector at KEK," ERL'13, Novosibirsk, p. 16 (2013).
- [4] M. Tobiyama et al., "Development of Button Electrode with Improved Time Response," BIW'08, Tahoe City, p. 205 (2008).
- [5] <http://www.gdfidl.de>
- [6] Y. Tanimoto et al., "Design of the cERL Vacuum System," IPAC'13, Shanghai, p. 3315 (2013).
- [7] <https://www.cst.com/Products/CSTPS>
- [8] P. Evtushenko et al., "Electron Beam Diagnostics of the JLab UV FEL," PAC'11, New York, p. 1446 (2011).
- [9] D. M. Gassner et al., "BNL Energy Recovery Linac Instrumentation," ERL'11, Tsukuba, WG4003 (2011).
- [10] T. Obina et al., "Optical Fiber Based Loss Monitor for Electron Storage Ring," IBIC'13, Oxford, p. 638 (2013).
- [11] H. Sagehashi et al., "Test of Detection Unit for the cERL High-speed Loss Monitor," the 11th Annual Meeting of PASJ, Aomori, SUP083 (2014) [in Japanese].
- [12] T. Obina et al., "Development of Compact Device Server with EPICS," the 11th Annual Meeting of PASJ, Aomori, MOOL08 (2014) [in Japanese].
- [13] Y. Honda et al., "Development of Bunch Length Monitor System at the Return Loop of KEK ERL Test Accelerator," the 11th Annual Meeting of PASJ, Aomori, SAP089 (2014) [in Japanese].